Inter-grid Transfer Influence on Transonic Flutter Predictions

A. Swift*and K.J. Badcock†

School of Engineering,

University of Liverpool,

L69 3BX, United Kingdom.

Computational Aeroelasticity requires a method to transfer displacements and forces between the fluid and structural grids. Several popular transformation methods are evaluated with respect to their sectional shape reconstruction properties, and the impact of these on flutter predictions. The test cases used are the Goland wing and a model commercial jet wing. The flutter predictions are computed using a fast eigenvalue tracing method. An approach to transformation for beam models is proposed based on defining additional information about the ribs to guide the choice of rigid sections.

I. Introduction

There are two main approaches to computational aeroelasticity. One approach uses a monolithic[1] scheme where the model equations are formulated to combine the fluid and structural equations into one system of equations. This requires a new solver to be written. The other approach is partitioned[2,3] where separate solvers are used for the fluid and structural systems and these are tied together using a transformation method, allowing the use of existing solvers. The most common approach is partitioned and is used in the current paper.

In the partitioned approach the aerodynamic loads need to be transferred to the structure and the structural deflections need to be transferred to the CFD mesh. This is complicated by the CFD requiring an accurate description of the surface geometry, and the structural model is usually defined on a simplified geometry, such as a plate, wing-box or beam. Despite adequately describing the important structural dynamics, this simplification produces the problem that there is a mismatch between the fluid and structural discretisations of the interface between the two models. This means that projection and extrapolation are usually required in addition to interpolation. Collectively the reconstruction of the fluid surface grid point locations and velocities from the structural model, and transfer of forces from the fluid surface grid to the structural grid, is referred to in this paper as transformation. There are several ways in which the shape of the wing can be altered in a non-physical manner (sectional and planform). Transformation methods should accurately recover the shape of the wetted surface, exact recovery of translation and rotation, conservation of energy, forces and moments. Reviews of transformation methods can be found in references.[4–7] Farhat et al[3] simplified the transfer problem of the F-16 fighter by defining both the CFD and structure on the same surface using an unstructured Euler CFD solver and a detailed structural model. However detailed structural models are not always available and can be difficult to tune to ground vibration tests.

The transformation methods can be grouped into two groups, local and global methods. Each have their own advantages and disadvantages. Local methods often depend on

*PhD Candidate

†Professor, SMAIAA, corresponding author. Tel. : +44(0)151 794 4847 , Fax. : +44(0)151 794 6841, Email : K.J.Badcock@liverpool.ac.uk

connectivity between the aerodynamic surface and the structural model and do not always give a smooth surface. However as the name suggests, they only use local information and have low memory requirements. Global methods are memory hungry and have non-local effects, but always provide a smooth surface.

The current paper considers an approach to the transformation that preserves key geometric properties of the aerodynamic shape. The method involves a consideration of the structural modelling assumptions, and the use of these assumptions to perform the reconstruction of the aerodynamic shape. It is argued that this approach is preferable to cloud of point methods that take no account of the structural assumptions.

This paper continues with a review of the formulation of the fluid, structural and aeroelastic stability solvers. Then several popular transfer methods are described, and the new method is detailed. Evaluation is made of the transfer methods for mode shape reconstruction and flutter prediction. Finally conclusions are given.

II. Formulation

A. Flow Solver

All the computations presented in this paper were performed using the Parallel Multi-Block (PMB) flow solver. A wide variety of problems have been studied using this code including cavity flows, delta-wing aerodynamics, rotorcraft problems, flutter and control surface buzz. For more information about the solver refer to Badcock et al.[8] The governing equations are discretised using a cell-centred finite volume approach combined with an implicit dual-time stepping method. In this manner, the solution marches in pseudo-time for each real time-step to achieve fast convergence. The discretisation of the convective terms uses Osher's upwind scheme. Monotone upstream-centred schemes for conservation laws (MUSCL) interpolation is used to provide nominally third order accuracy and the van Albada limiter is also applied to remove any spurious oscillations across shock waves. Central differencing is used to discretise the viscous terms, with the resulting non-linear system of equations generated being solved by integration in pseudo-time using a first-order backward difference. A Generalised Conjugate Gradient method is then used in conjunction with a Block Incomplete Lower-Upper (BILU) factorisation as a preconditioner to solve the linear system of equations, which is obtained from a linearisation in pseudo-time. A number of turbulence models are available in the solver as well as large-eddy simulation (LES) and detached eddy simulation (DES), however for the calculations presented in this paper the Euler equations were solved. Finally, meshes are moved in response to specified boundary locations using a spring analogy to move the block vertices, and the transfinite interpolation for the internal points in the block.

B. Structural Solver

The structure is modelled as linear and so it is possible to model the deformation as a sum of normal modes. The N degree of freedom structural model is written as a second order linear ordinary differential equation

$$[M]\ddot{\delta \mathbf{x}} + [C]\dot{\delta \mathbf{x}} + [K]\delta \mathbf{x} = \mathbf{f} \tag{1}$$

where $[M]$ is the mass matrix, $[C]$ is the viscous damping matrix and $[K]$ is the stiffness matrix, all of size $N \times N$. Here δx is the vector of time dependent displacements on the structural grid x, and f is the vector of time dependent external forces from the fluid, acting at the structural grid points. To calculate the undamped free vibration characteristics, Eq. (1) can be manipulated to an eigenvalue problem

$$[[A] - \lambda[I]]\Phi = 0 \tag{2}$$

where $[A] = [M]^{-1}[K]$ and $\lambda = \omega^2$. This can be solved to give the eigenvalues λ and mode shapes Φ. These mode shapes are mass normalised so that $[\Phi]^T[M][\Phi] = 1$.

Eq. (1) can be transformed into modal space which leads to the decoupled equations

$$\ddot{\eta}_i + \omega_i^2\eta_i = \Phi_i^T\mathbf{f} \tag{3}$$

for the i^{th} mode when damping is ignored. This equation can be solved for η_i using a Runge-Kutta scheme and the structural deformation with p modes retained is given by

$$\delta \mathbf{x} = \sum_{i=1}^{p} \Phi_i \eta_i \tag{4}$$

C. Schur Solver

The Schur solver[9] does a stability analysis based on the coupled system Jacobian, which includes the Jacobian of the CFD residual with respect to the CFD and structural unknowns. It is conventional in aircraft aeroelasticity for the structure to be modelled by a small number of modes, which leads to the number of the fluid unknowns being far greater than the structural unknowns. The Jacobian is partitioned into four blocks so that the Jacobian matrix has a large sparse block $\mathbf{A}_{ff}$ surrounded by thin strips for $\mathbf{A}_{fs}$ and $\mathbf{A}_{sf}$. The stability calculation is formulated as an eigenvalue problem, focussing on eigenvalues of the coupled system that originate from the uncoupled block $\mathbf{A}_{ss}$. The problem can be formulated as the structural problem modified by an interaction term, which depends on the eigenvalue itself and can be pre-computed. This formulation leads to a very efficient method of tracing the aeroelastic eigenvalues as functions of altitude, which in turn provides stability boundaries.

III. Transfer Methods

A. Types of Structural Model

Plate and beam structural models are used in the current work. The mode shapes are defined for these models in different ways. For plate models, the displacements $\delta\mathbf{x}_i$ are given directly at the structural grid points $\mathbf{x}_i$. For the beam models, the beam is defined by the points $\mathbf{x}_i$. In addition, we define directions along which the wing section is assumed to be rigid. These directions would be defined by the ribs in the wing structure. Hence, for each beam point $\mathbf{x}_i$, corresponding leading $\mathbf{x}_i^L$ and trailing $\mathbf{x}_i^T$ edge points define the rigid section. Then, the motion of this section is defined by the translation of the beam point, $\delta\mathbf{x}_i$, and the rotation of any point on the section $\delta\alpha_i$. The displacement of any point $\mathbf{y}$ on the section can then be derived as

$$\delta \mathbf{y} = \delta \mathbf{x}_i + R(\mathbf{y} - \mathbf{x}_i) \tag{5}$$

where A is the rotation matrix given by

$$R = \begin{bmatrix} \cos\delta\alpha_i & -\sin\delta\alpha_i \\ \sin\delta\alpha_i & \cos\delta\alpha_i \end{bmatrix}$$

The fluid grid is defined at $\mathbf{y}_i$, and the transformation problem is to define the displacements $\delta\mathbf{y}_i$ based on the definition of the displacements on the structural grid.

B. Transformation for Plate Model

First consider doing the transformation for a plate structural model. The fluid points are first projected onto the surface of the structural grid. Denote these points as $\mathbf{y}_i^P$, with a corresponding displacement $\delta\mathbf{y}_i^P$, referred to here as the projected displacement. The total displacement $\delta\mathbf{y}_i$ is the sum of the projected displacement and the displacement of the out-of-plane vector, denoted by $\delta\mathbf{y}_i^N$, i.e. $\delta\mathbf{y}_i = \delta\mathbf{y}_i^P + \delta\mathbf{y}_i^N$.

1. *Projected Displacement*

Different approaches are available for calculating the projected displacement:

1. Weighted Averages in a Triangle[10]

   Each projected point is associated with a triangle in the structural grid defined by three points $\mathbf{x}_1$, $\mathbf{x}_2$ and $\mathbf{x}_3$. Then, defining the vectors $\mathbf{a} = \mathbf{x}_2 - \mathbf{x}_1$, $\mathbf{b} = \mathbf{x}_3 - \mathbf{x}_1$ and $\mathbf{c} = \mathbf{y}_i^P - \mathbf{x}_1$, the following weighting factors are defined

$$w_1 = 1 - w_2 - w_3,$$

$$w_2 = \frac{|\mathbf{b}|^2(\mathbf{a.c}) - (\mathbf{a.b})(\mathbf{b.c})}{|\mathbf{a}|^2|\mathbf{b}|^2 - (\mathbf{a.b})(\mathbf{a.b})}$$

$$w_3 = \frac{|\mathbf{a}|^2(\mathbf{b.c}) - (\mathbf{a.b})(\mathbf{a.c})}{|\mathbf{a}|^2|\mathbf{b}|^2 - (\mathbf{a.b})(\mathbf{a.b})}.$$

Then

$$\delta \mathbf{y}_i^P = w_1 \delta \mathbf{x}_1 + w_2 \delta \mathbf{x}_2 + w_3 \delta \mathbf{x}_3$$

Two methods to do the association with projected points to triangles in the structural grid are described in reference.[2] For this work a hybrid method of fluid point assignment was used. The fluid points in the region of interpolation were assigned to the structural elements using an area-search and the points in the region of extrapolation were assigned using a nearest centroid approach. The limitation of this method is that the definition of the projected point displacements are only $\mathbf{C}^0$ continuous, with changing slopes between triangles.

2. Inverse Isoparametric Mapping[11]

Each projected point is associated with a quadrilateral in the structural grid, defined by the vertices $\mathbf{x}_1$, $\mathbf{x}_2$, $\mathbf{x}_3$ and $\mathbf{x}_4$. A pair of generalised coordinates (ξ, η) are defined on the quadrilateral using shape functions so that

$$\mathbf{x} = \Sigma_{i=1}^{4} N_i(\xi, \eta)\mathbf{x}_i$$

where the shape functions are defined as

$$N_1(\xi, \eta) = (1 - \xi)(1 - \eta)/4$$

$$N_2(\xi, \eta) = (1 + \xi)(1 - \eta)/4$$

$$N_3(\xi, \eta) = (1 + \xi)(1 + \eta)/4$$

$$N_4(\xi, \eta) = (1 - \xi)(1 + \eta)/4$$

Then for the projected coordinates $\mathbf{x}_p$, two equations can be solved for the corresponding values of (ξ^P, η^P). The projected point displacements are then evaluated as

$$\delta \mathbf{y}_i^P = \Sigma_{i=1}^{4} N_i(\xi^P, \eta^P)\delta \mathbf{x}_i$$

This method again only has continuity in the displacements as we go from quadrilateral to quadrilateral, but the interpolation is now bilinear which is an improvement on the weighted averages on triangles. Due to the shape functions the orientation (and therefore the ordering of the structural point) is now important. Again the definition of the point displacements is only $\mathbf{C}^0$ continuous.

3. Infinite Plate Spline[12]

Here the displacements of the projected point are calculated from a solution of the differential equations for a flat plate under an applied load. Note here that only the displacements normal to the plate (denoted here as δz) are calculated. The load is chosen to result in the known displacements at the structural points, and to display required behaviour as $|\mathbf{x}|$ becomes large. The displacement is written as

$$\delta z^P = a_0 + a_1 x + a_2 y + \Sigma_{i=1}^{N} F_i r_i^2 ln r_i$$

where N is the number of structural nodes, $r_i = |\mathbf{x}|$ and a_0, a_1, a_2 and F_i are all calculated from the equations

$$\Sigma_{i=1}^{N} F_i = 0$$

$$\Sigma_{i=1}^{N} F_i x_i = 0$$

$$\Sigma_{i=1}^{N} F_i y_i = 0$$

$$\delta z_i = a_0 + a_1 x_i + a_2 y_i + \Sigma_{i=1}^{N} F_i r_i^2 ln r_i.$$

This method provides smooth interpolation, however because IPS is derived from an infinite plate and then applied to a finite plate, this may cause IPS to produce non-smooth deformation at the edges. This is discussed in Sadeghi et al.[7] IPS also suffers when used for extrapolation, it has been documented that IPS creates distortions or oscillations in extrapolated regions.[13]

4. **Radial Basis Function[14]**

The radial basis function interpolant has the form

$$\delta\mathbf{y} = \sum_{j=1}^{M} \alpha_j \phi(|\mathbf{y}^P - \mathbf{x}_j|) + p(\delta\mathbf{y}) \tag{6}$$

where ϕ is the basis function and $\mathbf{x}_j$ are the locations of the centres of these basis functions. The linear polynomial $p(\mathbf{y})$ is used to ensure that translations and rotations are recovered. The coefficients α_i are found by requiring the exact recovery of the deflections at the structural node positions. The basis function used in this work was Wendland's C2 defined as $\phi(\|\{r\}\|) = (1 - \|\{r\}\|)_+^4\,(4\|\{r\}\| + 1)$ where $(.)_+ = max(0, .)$. A support radius is usually used which allows the control over the area of influence of each centre and is applied by $\phi(\|\{r\}\|/\rho)$ where ρ is the support radius. Norm-biasing is sometimes used to improve the result and is defined by $\|\{x\} - \{x_i\}\| = \sqrt{k_x(x-x_i)^2 + k_y(y-y_i)^2 + k_z(z-z_i)^2}$ where the coefficients k_x, k_y and k_z are changed to improve the interpolation result.

2. Out-Plane

For each of the four methods for calculating the projected displacement, the following method can be used to calculate the displacement of the out-plane component. As with the weighted average in triangles, each aerodynamic point is associated with a triangle in the structural grid. Using the notation defined above, the normal displacement vector is defined for the undeformed case as

$$\mathbf{d}_y = \mathbf{y}_i - \mathbf{y}_i^P$$

By definition of the projected point this vector is normal to a and b. Then, it is assumed that the displaced point $\mathbf{y}_i + \delta\mathbf{y}_i$ remains normal to the vectors $\mathbf{a}+\delta\mathbf{a}$ and $\mathbf{b}+\delta\mathbf{b}$, and that the magnitude is constant. This results in the perfect preservation of pure rotational motions. Define the normal vector after deformation as $\mathbf{d}_x = \pm(\mathbf{a} + \delta\mathbf{a}) \times (\mathbf{b} + \delta\mathbf{b})$ where the sign is chosen to orientate the normal in the same sense as the vector $\mathbf{d}_y$. This vector is then rescaled as

$$\mathbf{d}_x^* = \mathbf{d}_x \frac{|\mathbf{d}_y|}{|\mathbf{d}_x|}.$$

Finally, the out-plane displacement can then be written as

$$\delta\mathbf{y}_i^N = \mathbf{d}_x^* - \mathbf{d}_y.$$

C. Transformation for Beam Structural Models

For a beam structural model it is possible to use an intermediate step of defining a plate, so that any of the transformation methods described above can be used. The default way of doing this is to assume that the chord-wise sections have a fixed shape. A more general approach is to use points along the leading and trailing edges which define the ribs, and then base the intermediate plate definition on these points.

The IIM provides a straight forward approach, as follows. This method is referred to as the rigid section method.

1. **form a quadrilateral mesh defined by the beam, leading and trailing edge points**
2. **project the aerodynamic point onto this mesh**
3. **using the inverse iso-parametric mapping, calculate η in the element**
4. **calculate the beam point displacement and rotation for this value of η**
5. **using the origin coordinates of the aerodynamic point, apply Eq. 5 to calculate the displacement**

IV. Test Cases

There are some questions of interest that this paper aims to answer. First, what influence does C^0 continuity (as for CVT and IIM) have on the section shapes? Secondly what is the contribution of the out-of-plane component on the section shapes? Finally, what is the influence of any shape distortion on the flutter predictions. Two test cases are used to shed light on these questions. These are now described.

A. Goland Wing

The Goland wing, shown Fig. 1, is a rectangular wing that has a chord of 6 feet and a span of 20 feet. The aerofoil section is a 4% thick parabolic section. The CFD grid used was a coarse version with 35 thousand points and is block-structured using an O-O topology. This allows points to be focused in the tip region, which is the most critical region for the aerodynamic contribution to the aeroelastic response.

In this study three structural models were used. The original structural model is a wing-box that follows the description in reference[15] and includes a lumped mass tip store. A plate model is calculated from the wing-box by averaging upper and lower surface values onto a mid-plane using RBE3 elements. This model is referred to as the original plate.

The second model is an extension of the first. Points are added along the leading and trailing edges and also at the tip. These points are tied to the first plate model using RBAR elements. The element properties of the plate model have no rotational degrees of freedom, which are required by the RBAR elements for extrapolating the mode shapes. In order to recreate the mode shapes the points on the leading and trailing edges as well as the tip have their correct displacements extrapolated linearly using a Matlab script after being extracted from the NASTRAN output. Due to the positioning of the structural model inside the wing, the only areas of extrapolation are at the trailing edge and a small area at the tip. This model is referred to as the extended plate.

The final model was derived from the first model and is a beam stick model. The mid-plane points for the centre spar were chosen to be the beam points. The rotations at the beam points were calculated from the first and third spars using a Matlab script. The displacements of the leading and trailing edges were calculated in Matlab using Eq. 5. This model is referred to as the beam stick model (BSM). The structural models are shown in Figure 2.

The sections used in the shape comparisons are at 98% of the span and the position as well as the section is shown in Figure 1. This section is translated and rotated to the original orientation to allow for easier evaluation of the shape change introduced by the transformation.

B. MDO Wing

The second test case is the multi-disciplinary optimisation (MDO) wing,[16] this is a commercial transport wing with a span of 36m. The wing was optimised to fly at a certain altitude and Mach number and has a thick supercritical section. The CFD grid used was a coarse grid with 81 thousand points. The geometry and CFD grid is shown in Figure 3. For this work the in-plane mode is neglected.

In this study two structural models were constructed. The original structural model is a wing-box model and this was converted into two beam stick models. The MDO wingbox model has a set of points that resemble a beam that acts as the connection points for the lumped masses. The points are attached to the wing-box ribs though RBE3 elements, with one point with mass for each rib. These points were chosen to be the beam in the new beam model and the displacements and rotations were extracted directly from NASTRAN.

This serves as the basis for the two models. For the first model the points on the leading and trailing edges are chosen so that the rigid ribs are approximately perpendicular to the beam, matching the ribs on the wing-box model. The second model has the points on the leading and trailing edges so that the rigid ribs are parallel to the x-axis. These models are referred to as the perpendicular and parallel rib models respectively, and are shown in Fig. 4.

The section used in the shape comparisons is taken at 98% of the span perpendicular to the beam and the position as well as the section is shown in Fig. 3.

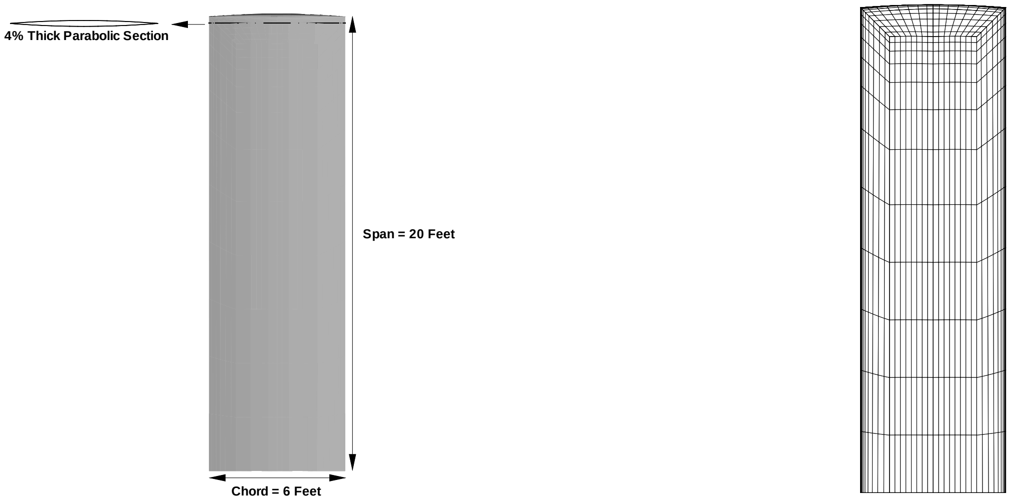

(a) Geometry (b) CFD Surface Mesh

Figure 1. Goland Wing Geometry and CFD Grid

V. Evaluation of Transfer - Shape

The transfer methods were implemented and are tested in this section in terms of the mapped mode shapes. To test the transformation methods shape comparisons are shown for several cases of increased complexity. The test section in each case is translated and rotated back to the original orientation to allow evaluation of the shape distortion introduced by the transformation.

A. Case 1 - In-plane

For this case the fluid grid is defined as a plane which is on the same surface as the structural grid and with the same planform as the Goland wing. The fluid grid is chosen to be much finer than the structural grids and this case tests the in-plane treatment of the transformation methods only. Both the original plate and extended plate are compared in this case. Fig. 5 shows the slice at 98% of the span for the third mode shape, which is the second torsion mode.

The CVT section exhibits a saw-tooth shape for both structural models, but passes through all of the NASTRAN points. This can be attributed to the lack of derivative continuity between structural elements. For the original plate, once the trailing edge of the structure has been reached, CVT extrapolates linearly. The IIM section passes through all of the NASTRAN points and provides linear extrapolation parallel to the element edges. The fact that IIM is only C^0 continuous does not show in the sections. IPS has trouble in the region of extrapolation for the original plate model where it flicks up to an unrealistically large deflection. Also throughout both structural models there are non-local extrapolation effects. There is a well known problem with IPS[6,7,13] that it cannot recreate rigid rotations. IPS performs much better when there is no extrapolation. The RBF support radius was chosen to be 1.0 in order for the first mode shape to pass through the NASTRAN points, and no norm-biasing was applied. The RBF result shows the same problem with extrapolation as IPS. The observed additional camber has been seen in other papers[17] (incorrectly attributed to fuselage interference) and Rendall et al[14] (where it was reduced by using norm-biasing).

This case highlights the differences between the local (CVT and IIM) and global (IPS and RBF) methods. The local methods exhibit a problem with slope discontinuity that the global methods do not suffer from. The global methods however fail to extrapolate realistically and have non-local effects due to extrapolation that is reduced when there

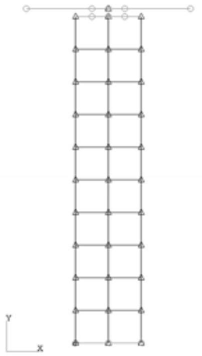

(a) Original NASTRAN Model

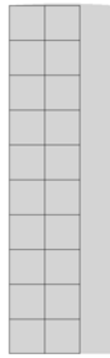

(b) Original Plate

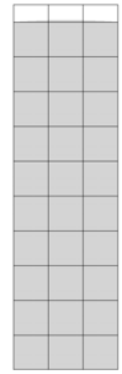

(c) Extended Plate

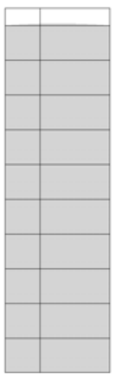

(d) Beam Stick Model

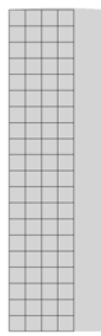

(e) Refined Original Plate

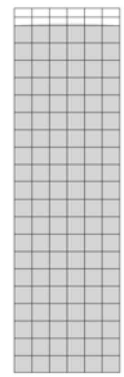

(f) Refined Extended Plate

Figure 2. Goland Wing Structural Models

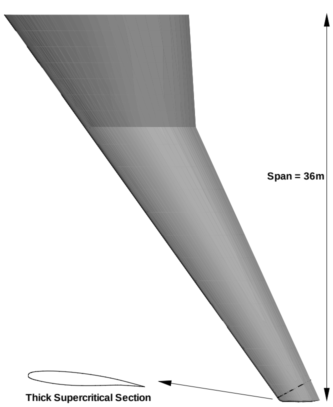

(a) Geometry

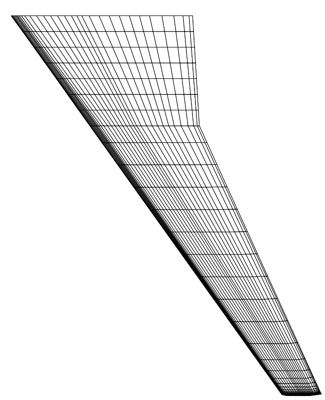

(b) CFD Surface Mesh

Figure 3. MDO Wing Geometry and CFD Grid

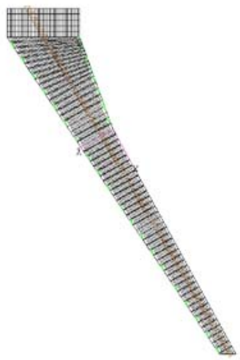

(a) Original NASTRAN Model

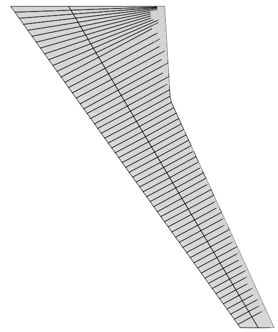

(b) Perpendicular Ribs

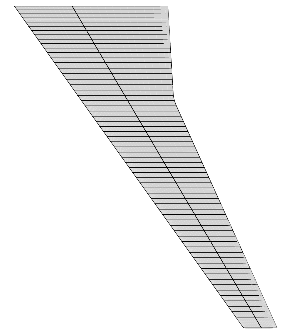

(c) Parallel Ribs

Figure 4. MDO Wing Structural Models

are no extrapolation regions. All the transformation methods performed better on the extended plate than the original plate for this reason.

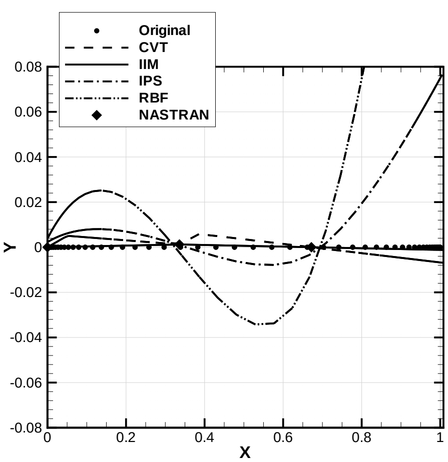

(a) Original Plate at 98% of the Span

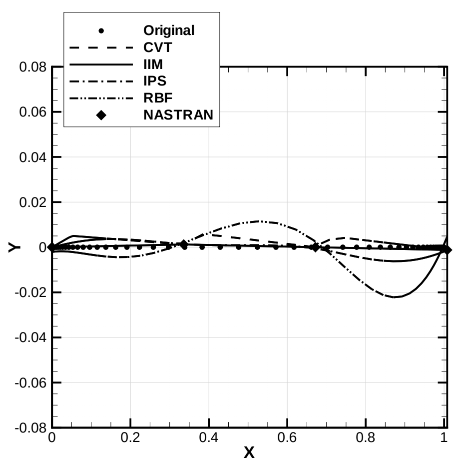

(b) Extended Plate at 98% of the Span

Figure 5. Case 1: Section at 98% span for the third Mode Shape, rigidly translated and rotated back to the original orientation.

B. Case 2 - Goland Wing In-plane

For this case the fluid grid is now defined on the correct wing profile, but the fluid points are projected onto the structural plane. The transformation methods are used to define the displacements at the projected points and then these displacements are applied without modification to the wing points. This tests the discrepancy introduced by failing to calculate the out-of-plane component. Again only the original and extended plate models are used.

Figure 6 shows a slice through the two plate models at 98% of the span for the third mode shape. All of the methods show the same behaviour as seen for case 1, but now on the wing section. CVT shows the C^0 continuity effect which leaves the aerofoil nonsmooth. Interestingly IIM shows no sign of this problem which may be due to higher order interpolation used within elements. RBF and IPS both display the same behaviour as case 1 with the trailing edge failing to be extrapolated correctly.

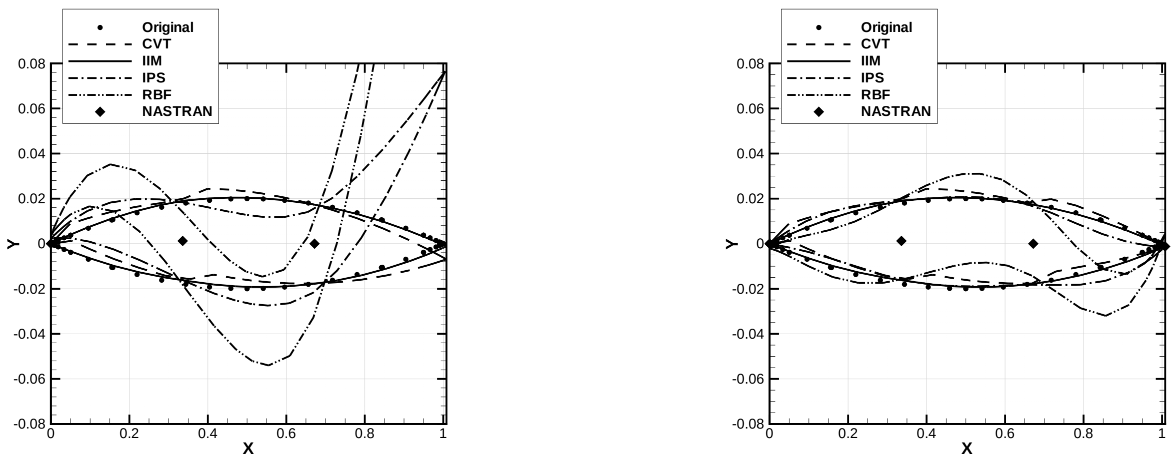

(a) Original Plate at 98% of the Span

(b) Extended Plate at 98% of the Span

Figure 6. Case 2: Section at 98% span for the third Mode Shape, rigidly translated and rotated back to the original orientation.

C. Case 3 - Goland Wing Out-of-plane

Next, the CVT out-of-plane component is added to the in-plane components calculated from each method. Fig. 7 shows the transformed slice. There is no significant change to the mode shapes between cases 2 and 3. It does seem to have the effect of thickening the section slightly. This is confirmed when the IIM result for case 2 is cross plotted with the IIM result for case 3, shown in Fig. 8. Since the out-of-plane components come from CVT there is a slight discontinuity introduced in the slope. It can be seen that the effect of the out-of-plane component is small.

To complete the picture of the performance of the plate transformation methods a refinement of the structural grid was undertaken, and is shown in Fig. 9 for the extended plate model. For the original and refined plate models each element was split into four elements and the displacements were linearly interpolated using a Matlab script. For all cases except IIM a significant improvement can be observed. For IIM there was no improvement shown, which implies that the IIM solution is already grid independent. For CVT the slope discontinuity problem persists, but its severity is less for both models. IPS is improved in the regions of grid refinement. The RBF follows the same story as it also benefits in the region of refinement and the extrapolation is also effected by the refinement. However although the improvement is significant for the RBF the sections are still the worst of the methods used.

D. Case 4 - Goland Wing Beam Stick Model

Finally the beam stick model is used and all the non-IIM methods calculate their out-of-plane contributions from the CVT method. The IIM results are from the rigid section method. The other results are defined using a grid defined by the beam points and the leading and trailing edge points that define the rigid sections. Figure 10 shows a slice at 98% for the third mode shape. The non-IIM methods are effectively using a coarsened extended plate model, since the BSM has one less row of structural points in the span-wise direction that corresponds to the trailing edge of the wing box in the other structural models. The sections are significantly worse as the trailing edge is approached for all methods except IIM. The rigid section results preserve the section very well.

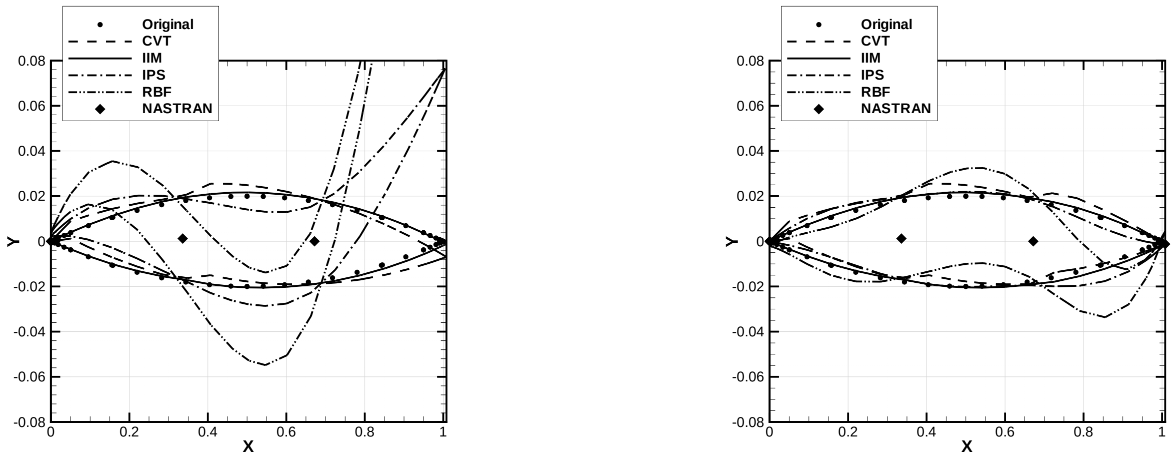

(a) Original Plate at 98% of the Span

(b) Extended Plate at 98% of the Span

Figure 7. Section at 98% span for the third Mode Shape, rigidly translated and rotated back to the original orientation.

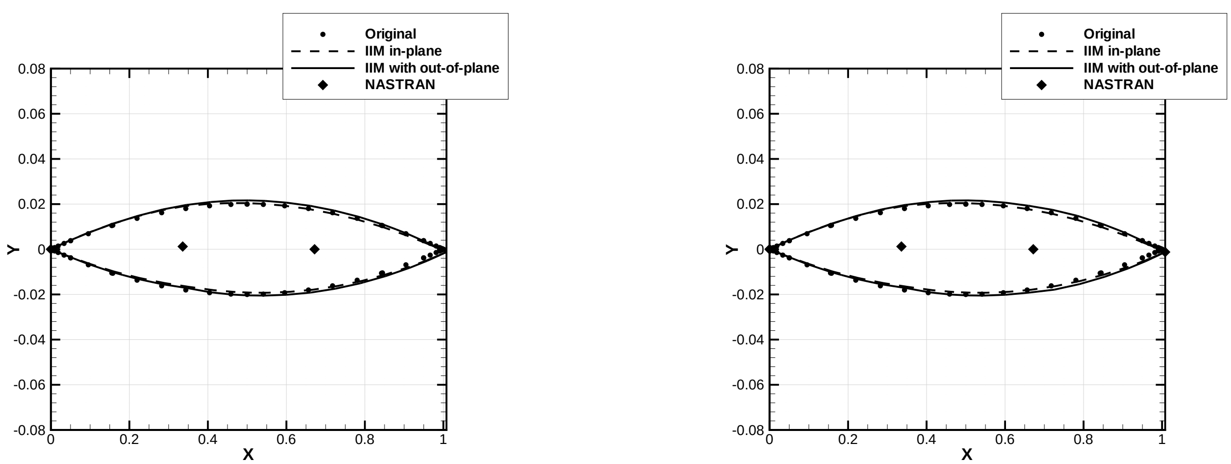

(a) Original Plate at 98% of the Span

(b) Extended Plate at 98% of the Span

Figure 8. Sections through the Mode 3 Mode Shape for IIM comparison for cases 2 and 3, rigidly translated and rotated back to the original orientation.

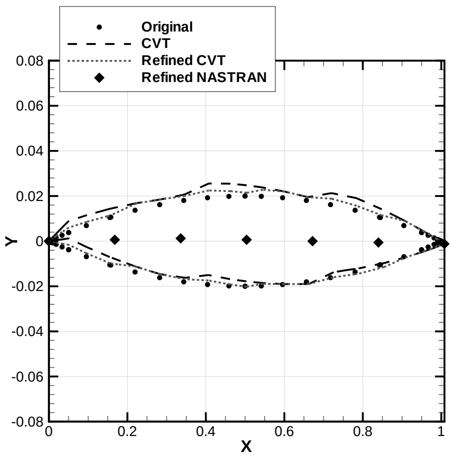

(a) CVT Extended Plate

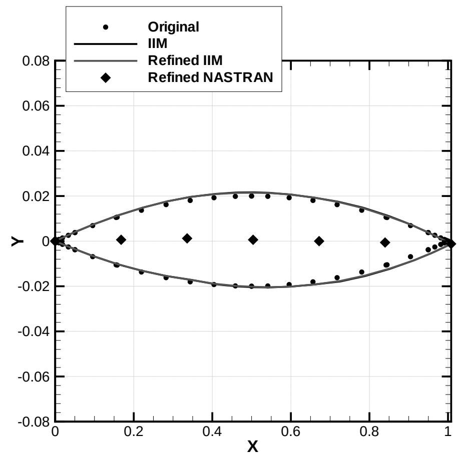

(b) IIM Extended Plate

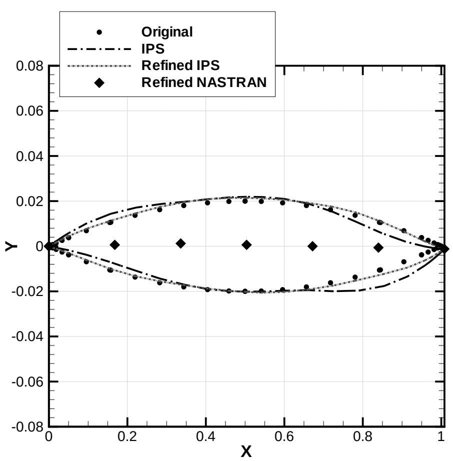

(c) IPS Extended Plate

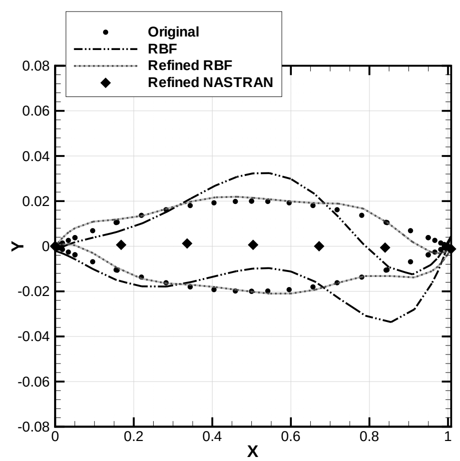

(d) RBF Extended Plate

Figure 9. Refined Plate Results for the extended plate model, rigidly translated and rotated back to the original orientation.

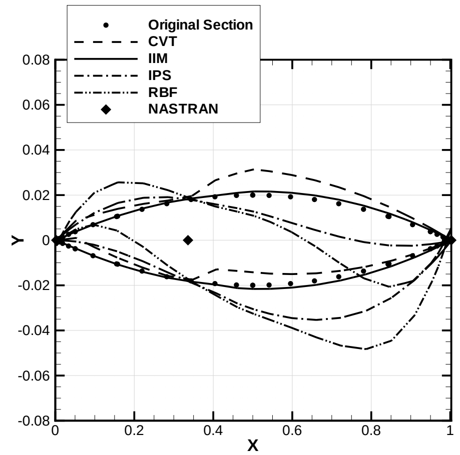

Figure 10. Case 4: Sections through the Mode 3 Mode Shape rotated and translated back to the original orientation.

E. Case 5 - MDO Wing

Next, results are shown for the two structural models of the MDO wing. The transformation methods are compared in terms of the vertical displacement calculated in Fig. 11. The rigid rib results are considered exact in this comparison since all methods only have access to the beam structural model, and the rigid rib method exploits this information exactly by design. For the two structural models CVT and the rigid ribs predictions are in close agreement. In contrast IIM and IPS shown a very non smooth behaviour which is associated with the out-of-plane displacements. Further, the predictions from the two structural models using CVT are compared. These shown that the parallel rib model leads to significantly larger trailing edge deflections for this mode.

F. Summary

- In-plane contributions usually dominate.
- CVT has discontinuities in slope because it is only C^0 continuous, but IIM does not suffer from this problem. This problem has a large influence on the section shapes.
- IPS and RBF are dependent upon the structural mesh density.
- The assumed rib orientation changes the sectional displacements.

VI. Flutter Evaluation

Having evaluated the influence of the transformation methods on the sectional shape, the impact of the distortions is now evaluated for the aeroelastic stability predictions. The Schur eigenvalue method is used to trace the aeroelastic eigenvalues as a function of altitude.

The Goland wing mode tracking at a Mach number of 0.80 and zero degrees incidence for all modes using CVT and the original plate model is shown in Figure 12. It can be seen that modes 1 and 2 interact, with mode becoming undamped between 10 and 15 thousand feet. The evaluation of the influence of the transformation methods is presented below for the real part of mode 1.

The mode tracking for the MDO wing at a Mach number of 0.85 and an incidence of one degree based on the beam model with perpendicular ribs, and with the CVT transformation used, is shown in Fig. 13. Modes 1,2 and 4 participate in the instability, with mode 1 going undamped first between 5000m below sea level and sea level.

First the predictions are compared for each method and the different structural models. These are shown for the Goland wing in Fig. 14. Consistent with the shape results presented above, the IIM shows the least spread of results between models. CVT and IPS show considerable spread, particularly where the interaction is strong as the mode

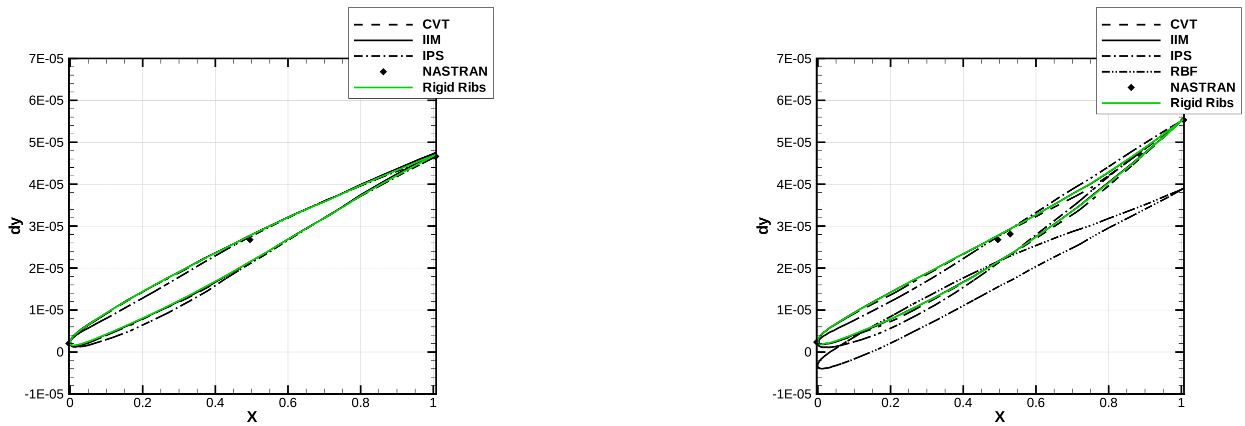

(a) Perpendicular Rib Model

(b) Parallel Rib Model

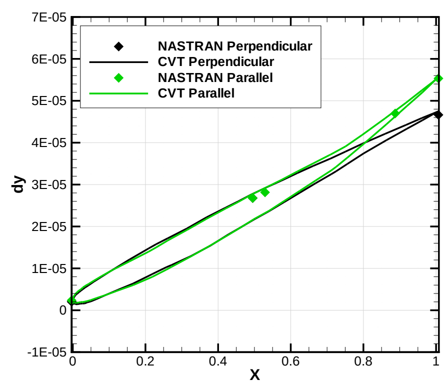

(c) Rigid Rib comparison of Parallel and Perpendicular Ribs

Figure 11. Case 5: Vertical Displacement of Sections for the Mode 5 Mode Shape.

becomes undamped. RBF shows a large spread, particularly for the original plate where extrapolation is involved. Next the results from different methods are compared for each model in turn and this is shown in Fig. 15. The predictions from IIM and CVT are close, with considerable differences between the global methods observed. These differences can be reduced by refining the plate in the structural model.

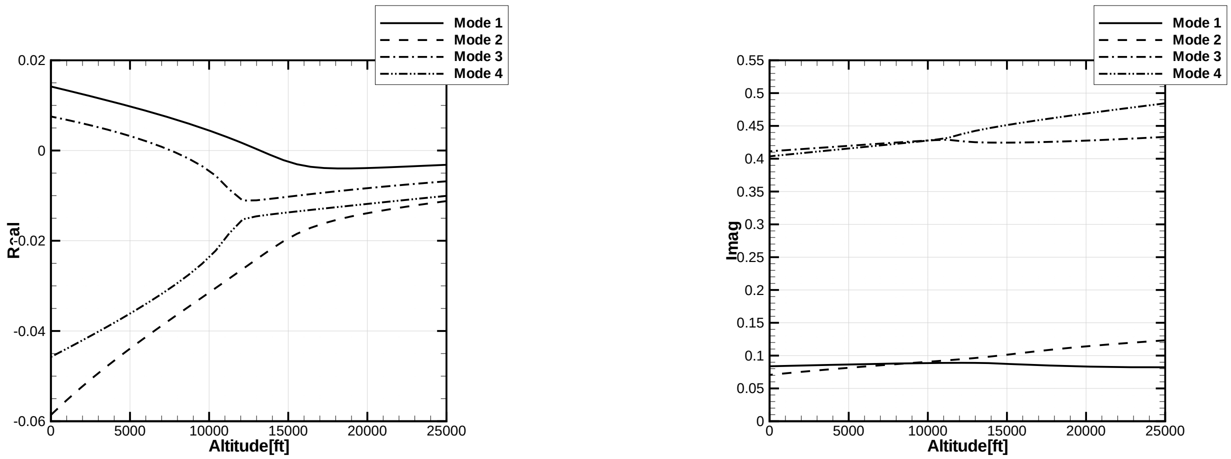

(a) Real Part (b) Imaginary Part

Figure 12. Goland Wing Mode Tracking for All Modes Using CVT

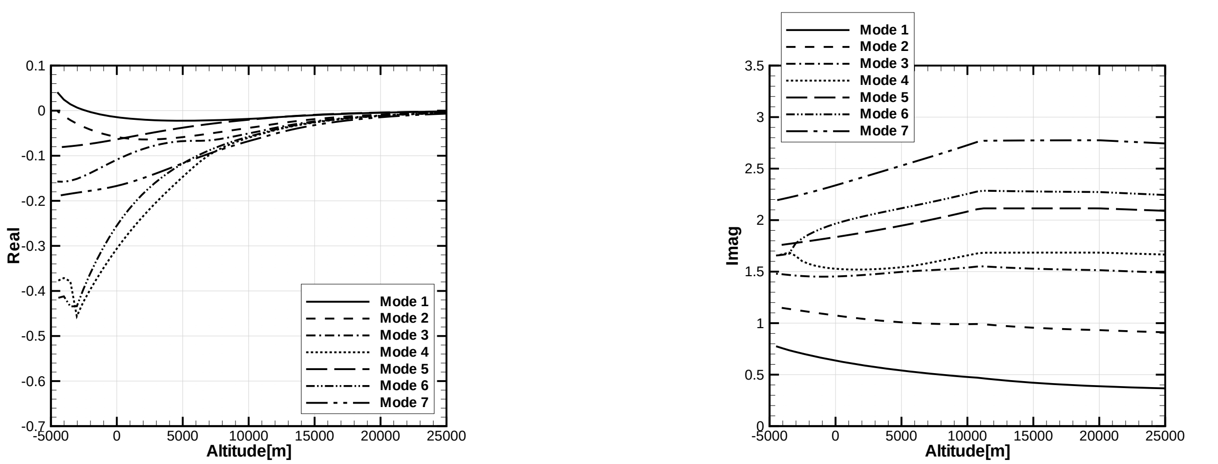

(a) Real Part (b) Imaginary Part

Figure 13. MDO Wing Mode Tracking for All Modes Using CVT

The MDO wing flutter mode tracking (in terms of the first mode, which goes undamped) is shown in Fig 16 for the different structural models using CVT. It is seen that there are significant differences in damping between the two structural models, even if the crossing at about the same altitude. The comparison of the predictions from the different transformation methods is shown in Fig. 17. The CVT and rigid rib predictions are very similar as expected from the displacement comparisons. There is a significant spread of results from the other methods, even more so than comes from the two structural models.

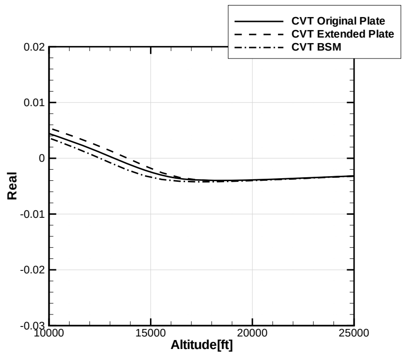

(a) CVT

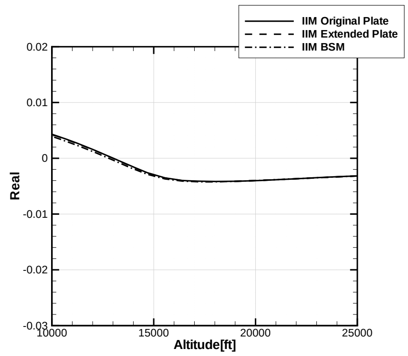

(b) IIM

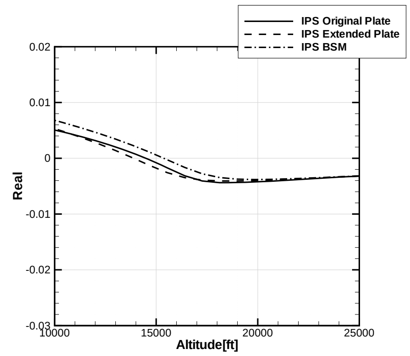

(c) IPS

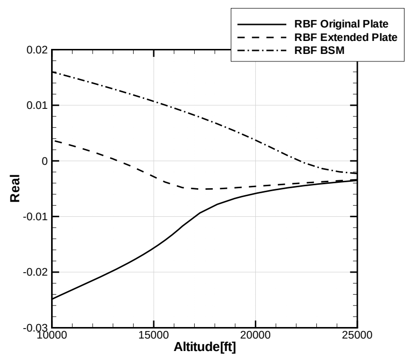

(d) RBF

Figure 14. Goland Wing Mode Tracking for Mode 1 for the different Structural Models (Real Part)

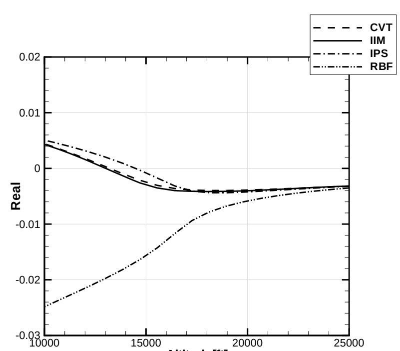

(a) Original Plate

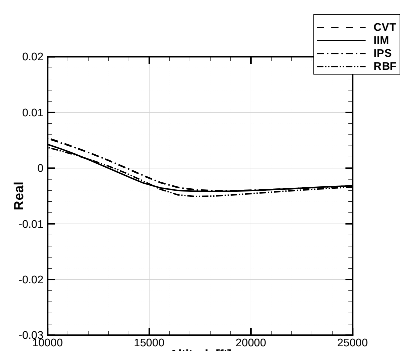

(b) Extended Plate

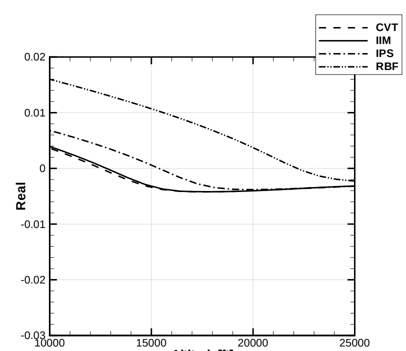

(c) BSM

Figure 15. Goland Wing Mode Tracking for Mode 1 for the different Structural Models (Real Part)

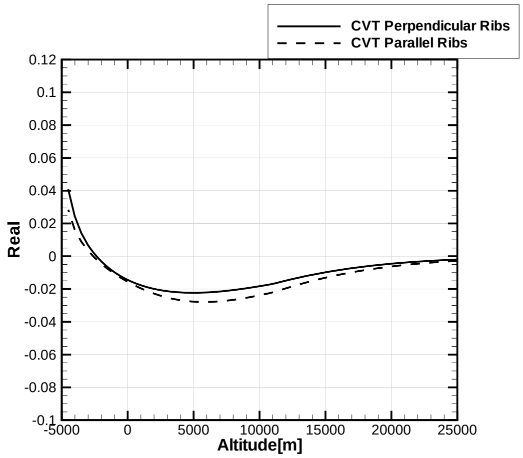

Figure 16. MDO Wing Mode Tracking for Mode 1 for the different Structural Models (Real Part) CVT

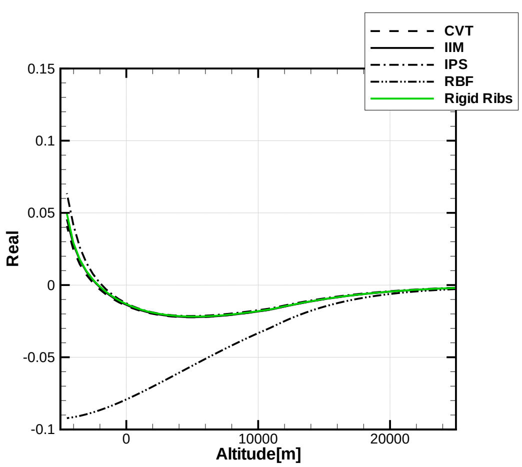

(a) Rigid Ribs Perpendicular to the Beam

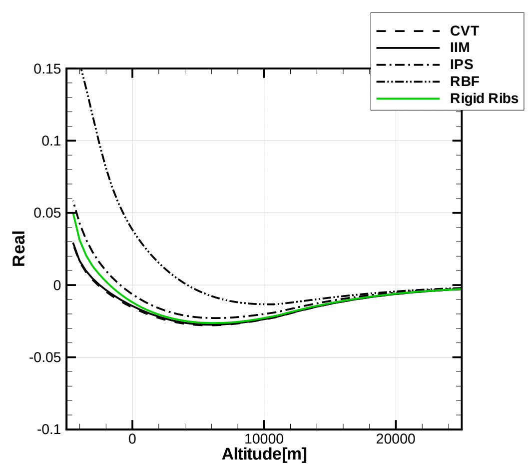

(b) Rigid Ribs Parallel to the x-axis

Figure 17. MDO Wing Mode Tracking for Mode 1 for the different Structural Models (Real Part)

VII. Conclusions

The performance of transformation methods for computational aeroelasticity was evaluated. Several common methods were compared for two test cases in terms of their predictions of the mode shapes on the CFD grid, and the influence of this on the aeroelastic damping. The lack of slope continuity from local methods was observed. In contrast the global methods were smooth, but required a finer structural grid to avoid oscillatory behaviour. The global methods also had problems in extrapolating beyond the support of the structural grid.

A new approach, referred to as rigid ribs, to preserving sectional shape when using beam structural models was proposed which requires the explicit definition of sections along which the wing profile is assumed to be rigid. The rib definitions are used to guide the association between fluid points and points on the beam.

Results suggest that the rigid rib method performs well, and that, despite the lack of derivative continuity inherent in the local methods used, the local methods provide more reliable flutter predictions.

VIII. Acknowledgements

This work was supported by the Engineering and Physical Sciences Research Council and BAE SYSTEMS.

References

[1]Hübner, B., Walhorn, E. and Dinkler, D., "A monolithic approach to fluid-structure interaction using space-time finite elements", *Computer Methods in Applied Mechanics and Engineering*, Vol. 193, 2004, pp. 2087-2104.

[2]Woodgate, M. A., Badcock, K. J., Rampurawala, A. M., Richards, B. E., Nardini, D., Henshaw, M.J.C., "Aeroelastic Calculations for the Hawk Aircraft Using the Euler Equations", *Journal of Aircraft* , Vol. 42, No. 4, 2005, pp. 1005-1012.

[3]Farhat, C., Geuzaine, P. and Brown, G., "Application of a three-field nonlinear fluid-structure formulation to the prediction of the aeroelastic parameters of an F-16 fighter", *Computers and Fluids*, Vol. 32, 2003, pp. 3-29.

[4]Smith, M. J., Hodges, D. H., and Cesnik, C. E. S., "Evaluation of Computational Algorithms Suitable for Fluid-Structure Interactions", *Journal of Aircraft* , Vol. 37, No. 2, 2000, pp. 282-294.

[5]Kamakoti, R. and Shyy, W., "Fluid-structure interaction for aeroelastic applications", *Progress in Aerospace Science*, Vol. 40, No. 8, 2004, pp. 535-558.

[6]Rampurawala, A. M., "Aeroelastic Analysis of Aircraft with Control Surfaces using CFD", Ph.D. thesis, University of Glasgow, 2006.

[7]Sadeghi, M., Lui, F., Lai, K. L., and Tsai, H. M., "Application of Three-Dimensional Interfaces for Data Transfer in Aeroelastic Computations", AIAA Paper 2004-5376, August 2004.

[8]Badcock, K. J., Richards, B. E., and Woodgate, M. A., "Elements of computational Fluid dynamics on block structured grids using implicit solvers", *Progress in Aerospace Sciences*, Vol. 36, 2000, pp. 351-392.

[9]Badcock, K.J. and Woodgate, M.A., Prediction of Bifurcation Onset of Large Order Aeroelastic Models, AIAA-2008-1820 in the proceedings of the 49^{th} Structural Dynamics and Materials Conference, AIAA, Schaumberg, Illinois, (2008).

[10]Goura, G. S. L., "Time Marching Analysis of Flutter using Computational Fluid Dynamics", Ph.D. thesis, University of Glasgow, 2001.

[11]Murti, V. and Valliappan, S., "Numerical Inverse Isoparametric Mapping in Remeshing and Nodal Quantity Contouring", *Computers and Structures*, Vol. 22, No. 6, 1986, pp. 1011-1021.

[12]Harder, R. L. and Desmarais, R. N., "Interpolation Using Surface Splines", *Engineering Notes*, February 1972, pp. 189-191.

[13]Smith, M. J. and Hodges, D. H. and Cesnik C. E. S., "An Evaluation of Computational Algorithms to Interface between CFD and CSD Methodologies", *U.S. Airforce Research Lab.*, WL-TR-96-3055, November 1995.

[14]Rendall, T. C. S. and Allen, C. B., "Unified Fluid-Structure Interpolation and MeshMotion using Radial Basis Functions", *International Journal for Numerical Methods in Engineering*, Vol. 74, 2008, pp. 1519-1559.

[15]Beran, P. S. and Khot, N. S. and Eastep, F. E. and Snyder, R. D. and Zweber, J. V., "Numerical Analysis of Store-Induced Limit-Cycle Oscillation", *Journal of Aircraft* , Vol. 41, No. 6, 2004, 1315-1326.

[16]Girodroux-Lavigne, P., Grisval, J. P., Guillemot, S., Henshaw, M., Karlsson, A., Selmin, V., Smith, J., Teupootahiti, E. and Winzell, B., "Comparison of static and dynamic fluid-structure interaction solutions in the case of a highly flexible modern transport aircraft wing", *Aerospace Science and Technology*, Vol. 7, 2003, pp. 121-133.

[17]Ahrem, R. and Beckert, A. and Wendland, H., "A Meshless Spatial Coupling Scheme for

Large-Scale Fluid-Structure-Interaction Problems", ***Georg-August-Universität*, Göttingen, Preprint Nr. 2005-19, 2006.**